Antarctic polar stratospheric clouds under temperature perturbation by nonorographic inertia gravity waves observed by micropulse lidar at Syowa Station

Takashi Shibata,[1] Kaoru Sato,[2] Hiroshi Kobayashi,[3] Masanori Yabuki,[4] and Masataka Shiobara[2]

[1]   Type II polar stratospheric clouds (PSCs) were observed by micropulse lidar (MPL) at Syowa Station in the Antarctic on 30 June and on 1 July 2001. The vertical profiles of the PSCs had a wavy structure that was synchronized with the temperature fluctuations. A wave analysis using radiosonde data shows that the wavy fluctuations were associated with an inertia gravity wave that was not forced by ground topography, but probably by a spontaneous adjustment in association with synoptic-scale wave-breaking processes in the upper troposphere. It is suggested that the observed PSCs were generated under the low-temperature conditions induced by these waves and that such gravity waves generated by spontaneous adjustment of large-scale fields can be more important to the formation of PSC particles, in both the Antarctic and Arctic stratosphere, than topographically forced gravity waves, because the former are not fixed to the ground topography.   *INDEX TERMS:* 0305 Atmospheric Composition and Structure: Aerosols and particles (0345, 4801); 0320 Atmospheric Composition and Structure: Cloud physics and chemistry; 0340 Atmospheric Composition and Structure: Middle atmosphere—composition and chemistry; 3334 Meteorology and Atmospheric Dynamics: Middle atmosphere dynamics (0341, 0342); *KEYWORDS:* polar stratospheric clouds, inertia gravity waves, micropulse lidar

1. Introduction

[2]   Polar stratospheric clouds (PSCs) composed of ice particles are the main atmospheric constituents that provide surfaces for the heterogeneous chemical reactions that lead to ozone destruction in the Antarctic stratosphere. Denitrification, which is a process needed for ozone destruction, is caused by the gravitational sedimentation of the ice particles that have grown large enough under the low-temperature conditions of the Antarctic stratosphere in the winter season [e.g., *Solomon*, 1999].

[3]   The ice particles can exist at a temperature lower than the frost point (T_{ice}). Some studies show that the ice particles are formed at $2-4$ K lower temperature below T_{ice} (T_{ice-nu}) [*Zhang et al.*, 1996; *Tabazadeh et al.*, 1997; *Koop et al.*, 1998; *Carslaw et al.*, 1999]. The low-temperature ($<T_{ice-nu}$) region in the stratosphere is formed on synoptic scale over Antarctica in midwinter. The ice particles have been observed

widely in this low-temperature region. However, as far as in terms of synoptic scale, the temperature is higher than T_{ice-nu} over Antarctica at the beginning of winter, and is usually higher than T_{ice} in the Arctic stratosphere all through winter. Further cooling by smaller-scale atmospheric motion is needed for the formation of ice particles in these higher synoptic-scale-temperature conditions. PSC particles composed of ice were often observed under lee wave perturbation induced by the Scandinavian mountains. In that study, it was deduced that type II PSCs (ice particles) observed by lidar downstream from the mountains were formed by the low temperature ($<T_{ice-nu}$) associated with the lee waves [*Carslaw et al.*, 1998a, 1998b].

[4]   Denitrification has also been observed in the Arctic stratosphere as in the Antarctic [*Sugita et al.*, 1998; *Waibel et al.*, 1999]. A similar process of ozone destruction seems to work over the Arctic as that over the Antarctic. However, since it is rare that the stratospheric temperature drops lower than T_{ice}, ice particles are not the main type of the PSC particles over the Arctic. The Arctic PSCs are particles mainly composed of a super cooled ternary solution (STS) of $HNO_3/H_2SO_4/H_2O$, which form under the higher temperature conditions found in the Arctic stratosphere [e.g., *Shibata et al.*, 1999]. The formation temperature of STS particles (T_{STS}) is $3-4$ K higher than T_{ice}. The STS particles do not grow large enough for gravitational sedimentation to cause significant denitrification. A small number of solid

[1]Graduate School of Environmental Studies, Nagoya University, Nagoya, Japan.
[2]National Institute of Polar Research, Tokyo, Japan.
[3]Department of Ecosocial System Engineering, Yamanashi University, Yamanashi, Japan.
[4]Center for Environmental Remote Sensing, Chiba University, Chiba, Japan.

particles composed of nitric acid hydrates (NAH) are also often observed in the Arctic stratosphere by lidar even at temperatures higher than T_{ice} or T_{STS} [*Shibata et al.*, 1999; *Shibata*, 1999]. *Fahey et al.* [2001] observed large-size particles ("rock particles") containing HNO_3 in the winter Arctic stratosphere. They suggested that these rock particles efficiently remove HNO_3 from the stratosphere with their large sedimentation velocity. Thus, solid NAH particles play an important role in the ozone chemistry over the Arctic. However, their formation mechanism is still not clear.

[5]   Several mechanisms have been proposed to explain the formation of the solid PSC particles in the relatively warm environment of the Arctic stratosphere (see the review of *Carslaw et al.* [1999]). Some of them are the formation of the NAH particles at a temperature lower than the equilibrium temperature of nitric acid trihydrate (NAT) (T_{NAT}) without assuming the formation of ice particles, where T_{NAT} is 7–8 K higher than T_{ice}. *Tabazadeh et al.* [1996], for example, suggested that solid NAH particles might nucleate in air parcels whose temperature has been kept below T_{NAT} for more than ~1 day. The other mechanisms are formation of NAH particles from ice particles. These, therefore, need a temperature below T_{ice-nu} to form ice particles before the formation of solid NAH particles. One of the later mechanisms proposed by a research group at the Max Plank Institute is that the ice particles are formed under lee wave perturbation, then the solid NAH particles are formed from the ice particles when the temperature rose above T_{ice} [*Carslaw et al.*, 1998a, 1998b, 1999]. They estimated the formation of NAH solid PSC particles in the Arctic by model calculations, and indicated that the temperature perturbation induced by orographic waves may be an important source of solid particles on the synoptic scale.

[6]   Mesoscale perturbations in the stratosphere are induced not only by surface topography but also by instabilities in the atmosphere. *Yoshiki and Sato* [2000] analyzed gravity waves based on operational radiosonde observations from 33 stations in polar regions over a 10 year period. The propagation characteristics and the correlation of the gravity wave energy with the background wind suggested that the analyzed gravity waves in the Arctic are mainly forced by topography, whereas some sources in the Antarctica may exist in the stratosphere. *Sato* [2000] also discussed possible sources of the gravity waves in the polar middle atmosphere.

[7]   Although the directly observed PSCs formed by the mesoscale dynamical perturbation have been only by the lee waves over Scandinavia, the current study shows a case of type II (ice) PSC formation over the Antarctic in association with nonorographic inertia gravity waves. The PSCs were observed by micropulse lidar, and the nonorographic inertia gravity waves were observed by routinely launched operational radiosonde soundings by balloon. This kind of gravity wave probably plays an important role in the ozone depletion chemistry over both polar regions, since, unlike lee waves, such gravity waves can be generated anywhere and propagate horizontally.

2.   MPL-Observed PSCs

[8]   The PSCs were observed over Syowa Station (69.0°S, 39.5°E), Antarctica by a micropulse lidar (MPL) system. MPL is an eye-safe and maintenance-free portable lidar system developed by *Spinhirne* [1993]. The MPL used in this study was manufactured by SESI, USA and is based on the Spinhirne's original MPL [*Lee et al.*, 1997]. It uses a diode laser pumped Nd:YLF laser. Wavelength, output energy, and pulse repetition of the laser were 523.5 nm, 7 μJ/pulse, and 2500 Hz, respectively. The MPL can receive a return signal from a 60 km range with a range resolution of 30 m. The diameter of the receiving telescope is 20 cm. The field of view of the receiver is 100×10^{-6} radians. Data were acquired in one-minute pulse-integration mode. This MPL was installed at Syowa Station in January 2001 to observe tropospheric aerosols and clouds there, but it can also be used for PSC observations when well-grown type II PSCs appear in the stratosphere [*Shiobara et al.*, 2001].

[9]   Figure 1 shows the backscattering ratio (*BR*) observed on 30 June 2001. *BR* is defined as

$$BR = \frac{\beta_{Ray} + \beta_{Mie}}{\beta_{Ray}}, \qquad (1)$$

where β_{Ray} and β_{Mie} are the backscattering coefficient of Rayleigh and Mie scattering, respectively. *BR* minus 1 is proportional to the mixing ratio of PSC particles. The PSCs began to appear on 29 June, and showed maximum backscatter around 0200-1100LT (LT = UT + 0300) on 30 June.

[10]   The *BR* in Figure 1 shows a wavy structure with two to four layers. The altitudes of the backscatter-peaks descended with time. The distance between the heights of the *BR* peaks (vertical wavelength of the PSCs' wavy structure) was 3–4 km. It took about 24 hours for the height of the *BR* peak to descend this distance (i.e., the period of the PSCs' wavy structure).

[11]   Figure 2 shows the temperature profile observed by operational radiosonde soundings at 1500LT(12UT) on 30 June at Syowa Station. This temperature profile also shows a wavy structure between the altitude of 10 and 25 km. The profile of T_{ice} is also shown in Figure 2, as calculated by assuming a water vapor mixing ratio of 5 ppmv. Figure 3 shows the profiles of T-T_{ice} and *BR*. The atmospheric temperature was lower than T_{ice} by more than four degrees. The altitudes of the T peaks roughly coincided with the altitude of the minimums in T-T_{ice}, suggesting that the low temperature and the enhancement of *BR* were induced by the perturbation from the same wave activity.

[12]   For type I PSCs over the Arctic, a maximum *BR* value of 8 has been observed at the altitude where the temperature was almost at T_{ice} [*Shibata et al.*, 1997]. Since depolarization is not measured by MPL, the PSCs observed by MPL cannot be classified by the conventional method, which compares backscatter and depolarization [e.g., *Shibata et al.*, 1999]. Although there is still possibility that the observed PSC particles are composed of STS, the backscattering ratio larger than 10 indicates the particles contain higher amount of water than STS [*Shibata et al.*, 1997], and it is highly probable that the particles were frozen at the temperature lower than T_{ice-nu}. Therefore, the PSCs observed by MPL were probably the type II composed of ice particles.

3.   Characteristics of the Inertia Gravity Wave

[13]   A similar wavy structure in the temperature profile is also seen in the horizontal wind profiles shown in Figure 4
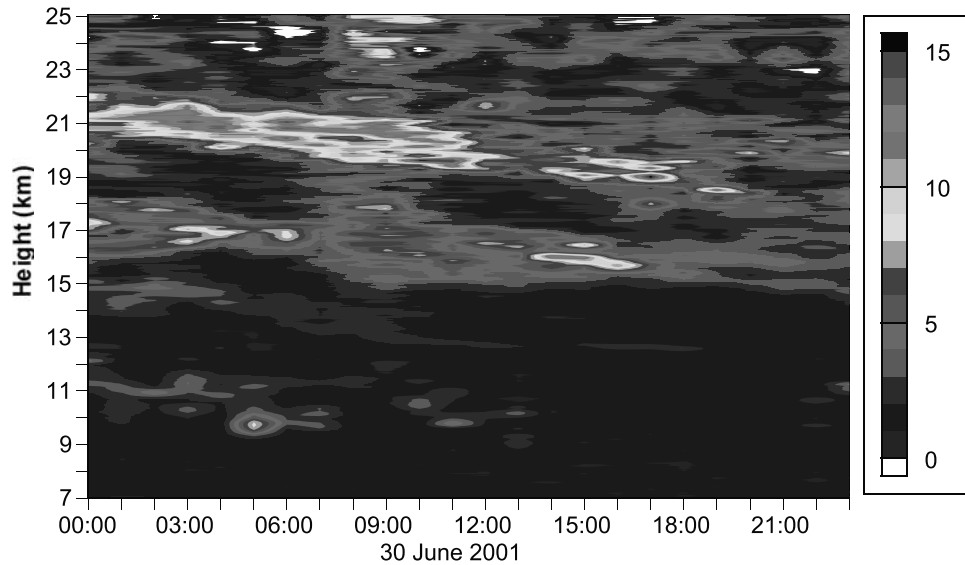
Figure 1. Backscattering ratio by MPL at 523 nm from 00 UT to 23 UT on 30 June 2001. See color version of this figure at back of this issue.

(the same sonde data as in Figure 2). There are two possible phenomena for horizontal wind fluctuations having such small vertical scales (about 4 km). These are gravity waves and filaments. However, judged from the fact that the fluctuations with similar scales are seen in temperature profiles, it is highly probable that these fluctuations are due to internal gravity waves having large vertical displacements. Thus under the assumption of gravity waves, we performed a hodograph analysis to estimate wave parameters. The validity of this assumption can be confirmed by coincidence of estimates of particular parameters obtained from independent methods.

[14] To extract fluctuation components, we applied a band-pass filter having cutoff lengths of 2 and 8 km to the original profiles. The background fields were extracted using a low-pass filter with a cutoff length of 8 km. The estimation was made for the height range of $16.6–20.2$ km where about one wavelength is clearly seen and the mean wind can be regarded as constant. Vertical profiles of zonal (u') and meridional (v') wind fluctuations and buoyancy divided by the Brunt-Väisälä frequency N (i.e. $T'g/\overline{T}N$) are
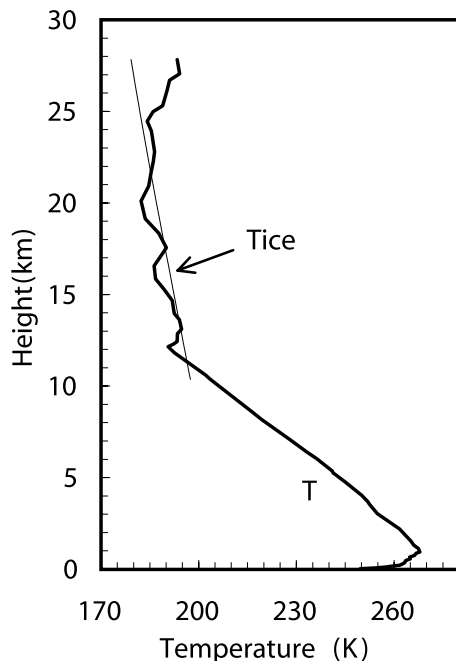
Figure 2. Temperature (solid line) over Syowa at 1500 LT (12 UT) on the 30 June 2001 observed by operational radiosonde sounding. T_{ice} (thin line) calculated by assuming 5 ppmv of H_2O is also shown.
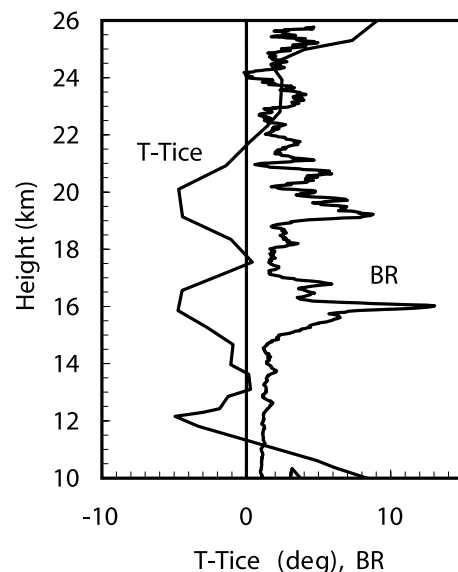
Figure 3. T-T_{ice} from the data shown in Figure 2, and BR at 1500LT (12UT).
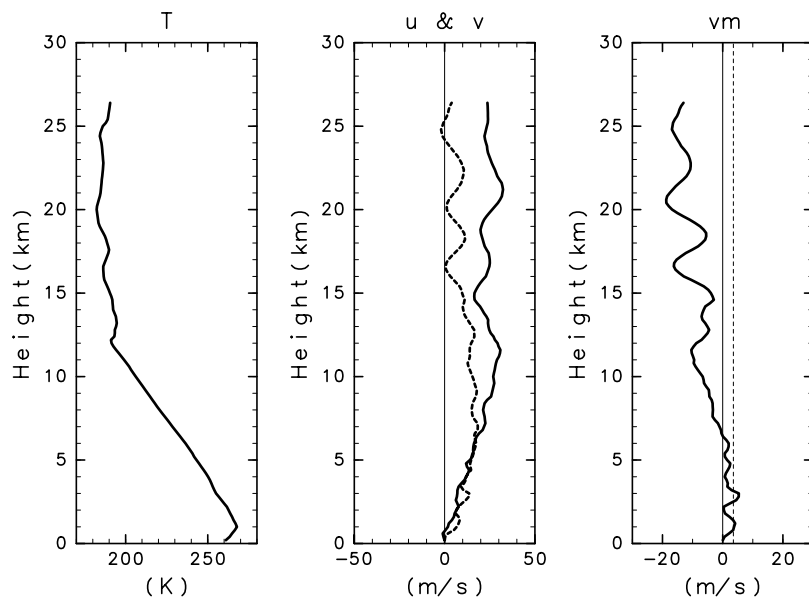
Figure 4. Left and center panels show, respectively, the vertical profiles of temperature and the vertical profiles of zonal (solid line) and meridional (dashed line) winds over Syowa at 1500 LT (12 UT) on 30 June, 2001 observed by radiosonde (the same sonde data as in Figure 2). The right panel shows a vertical profile of the horizontal wind component parallel to the wavenumber vector of the gravity wave (solid line), and the ground-based phase velocity estimated from the wave parameters (dashed line).

shown as solid curves in Figure 5. These are fitted into the following sinusoidal shapes;

$$u' = V_1 \cos\theta - V_2 \sin\theta, \tag{2}$$

$$v' = V_1 \sin\theta + V_2 \cos\theta, \tag{3}$$

and

$$\frac{T'g}{TN} = -FV_2, \tag{4}$$

where V_1 and V_2 are horizontal wind fluctuations parallel and perpendicular to the horizontal wavenumber vector, θ is

the angle of the wavenumber vector (counterclockwise from the eastward direction), and F is a real constant. The wind fluctuations V_1 and V_2 are expressed as

$$V_1 = a\cos(mz + \varphi), \tag{5}$$

and

$$V_2 = b\sin(mz + \varphi), \tag{6}$$

where a and b are wind amplitudes parallel and perpendicular to the horizontal wavevector, m is the vertical
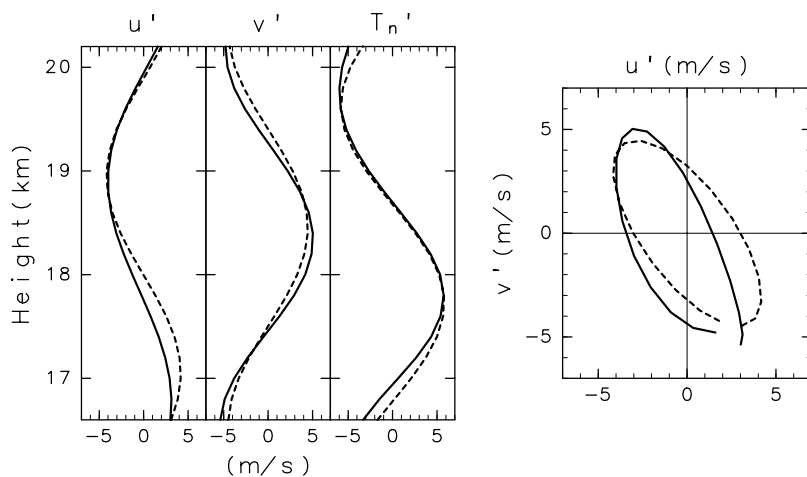
Figure 5. Left panel: Solid curves show vertical profiles of observed zonal and meridional wind and temperature fluctuations ($T'g/TN$); dashed curves show the results of the hodograph fitting. Right panel: Solid curve shows the observed hodograph of the wind fluctuations for the height region of 16.6–20.2 km; dashed curve shows the result of the PSC fitting; arrow shows direction of the horizontal wave number vector.

wavelength, z the height, and φ the phase at the ground. The results of the fitting are shown by dashed curves in Figure 5.

[15] According to the inertial gravity wave theory, the intrinsic frequency (the frequency relative to the mean wind) $\hat{\omega}$ is related to a and b as

$$b/a = f/\hat{\omega}, \tag{7}$$

where f is the inertial frequency, which is negative (positive) in the Southern (Northern) Hemisphere. Thus, from the ratio of a to b estimated by the fitting, we can obtain the intrinsic frequency $\hat{\omega}$ and the direction of the horizontal wavenumber vector with an ambiguity of 180°. The dispersion relation of the inertial gravity wave is

$$\frac{k^2}{m^2} = \frac{\hat{\omega}^2 - f^2}{N^2 - \hat{\omega}^2}, \tag{8}$$

where k is the horizontal wavenumber and N is the Brunt-Väisälä frequency. Thus, using this equation, we can estimate the horizontal wavenumber k. Moreover, from the polarization relation of inertia gravity waves, the temperature fluctuation amplitude can be estimated by the horizontal wind amplitude and horizontal and vertical wavenumbers in the following equation.

$$F = -\frac{Nk}{mf} \equiv F_{\text{est}}. \tag{9}$$

(see *Gill* [1982] for a reference). It is also worth noting that the ambiguity of the horizontal wavenumber vector can be resolved by equation (9) [see also *Sato and Yamada*, 1994; *Sato*, 2000].

[16] The wave parameters estimated with this method are as follows: horizontal wavelength (λ_h), 290 km; vertical wavelength (λ_z), 3.8 km; ground-based wave period (τ), 23 h; intrinsic wave period ($\hat{\tau}$), 5.5 h; horizontal wind amplitude parallel to the wavenumber vector (a), 5.6 ms^{-1}; horizontal wind amplitude perpendicular to the wavenumber vector (b), 2.4 ms^{-1}; F in equation (4), 2.4; and F_{est} in equation (9), 2.1. The hodograph and the fitted ellipse, as well as the direction of the horizontal wavenumber vector, are shown in Figure 5. It is clear that the fitting analysis was successful. It is worth noting that good correspondence between F and F_{est} assures the validity of the gravity wave assumption. The rotation of the hodograph is anti-clockwise, indicating that the inertia gravity wave propagates energy upward. It is also worth noting that the horizontal wavelength of 290 km is sufficiently long to be detected by MPL with the horizontal width of the field of view of ~2 m at 20 km in altitude.

[17] The estimated ground-based wave periods as well as vertical wavelength nicely matched the characteristics of the observed PSC layers. Thus it is likely that the PSC layers were modulated by this inertia gravity wave. The right panel of Figure 4 shows the vertical profile of the background wind in the direction of the horizontal wavenumber vector. The ground-based phase velocity c estimated from the wave parameters was 3.6 ms^{-1}, and is shown by the dashed line in the same figure. Although c was small, this inertia gravity wave could not have been a topographically forced wave, because there were critical levels below the height of 6 km.
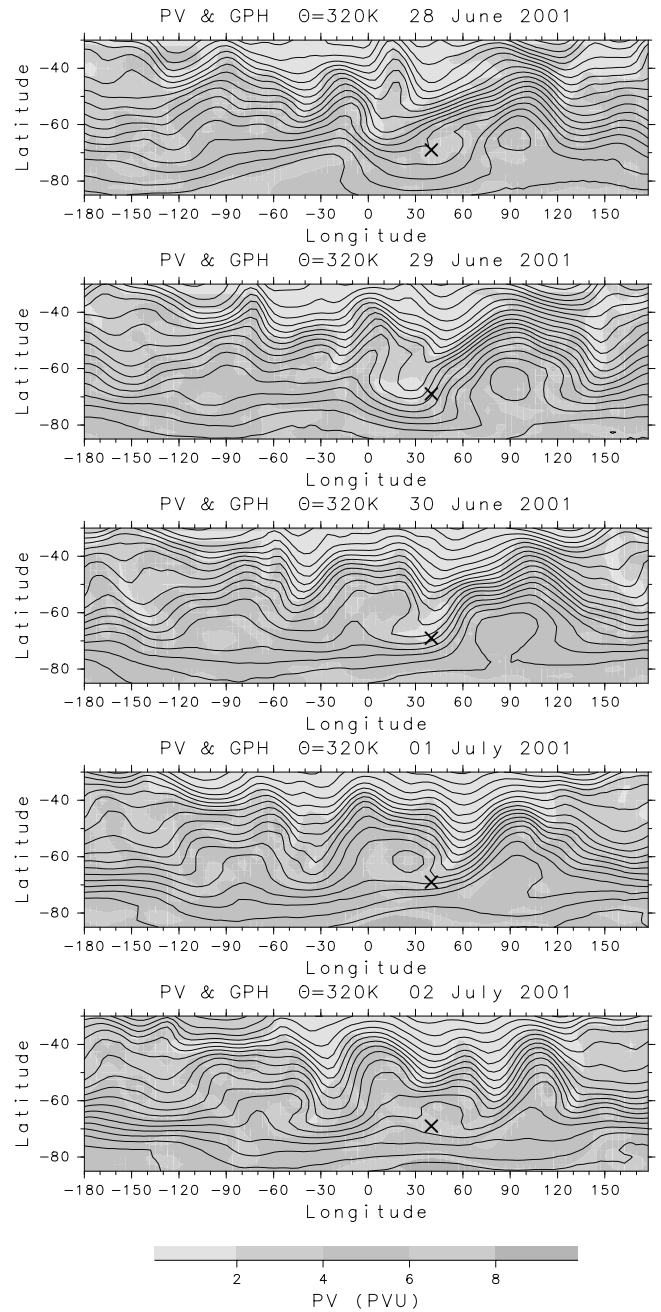
Figure 6. Time series of horizontal maps of the geopotential height at a pressure level of 215 hPa (contours) and the potential vorticity (PV) at a potential temperature level of 320 K (color), for the time period of 29 June to 2 July 2001, based on UKMO assimilation data. Contour intervals are 100 m. The pressure and potential temperature levels correspond roughly to a height of 10 km. The location of Syowa Station is denoted by a cross. See color version of this figure at back of this issue.

As shown by *Yoshiki and Sato* [2000], it is likely that the inertia gravity wave has a source in the upper troposphere or the stratosphere.

[18] Figure 6 shows a time series of horizontal maps of the geopotential height at a pressure level of 215hPa
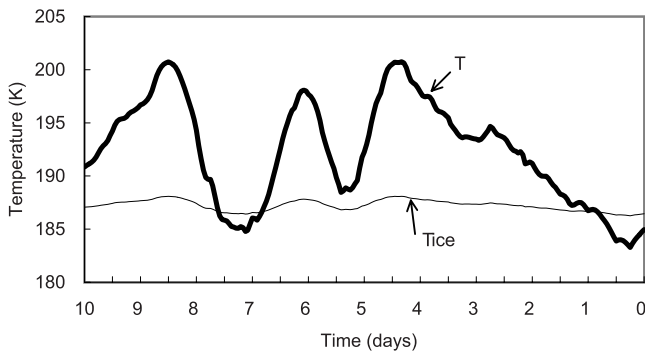
Figure 7. Temperature history of the air parcel at 20 km over Syowa at 1500 LT on 30 June 2001 calculated by back trajectory using the objective analysis data of the Japan Meteorological Agency. T_{ice} is also shown by a thin line.

(contours), along with the potential vorticity (PV) at a potential temperature level of 320K (color), for the time period of 29 June to 2 July 2001, based on UKMO assimilation data [*Swinbank and O'Neill*, 1994]. The pressure and potential temperature levels correspond roughly to a height of 10 km. The location of Syowa Station is denoted by a cross mark. A synoptic-scale ridge passed near Syowa Station around 30 June 2001. The time evolution of the PV pattern observed in Figure 6 indicates that the ridge structure was nonlinear and wave breaking has occurred. Gravity wave generation with such nonlinear processes of baroclinic waves was shown observationally by *Sato* [1989] and numerically by *O'Sullivan and Dunkerton* [1995]. Thus, it is likely that the gravity wave was generated by the spontaneous adjustment associated with the nonlinear processes in the upper troposphere.

4. Discussions

[19] Figure 7 shows the temperature history of the air parcel (or of the PSC) at 20 km over Syowa at 1500LT on 30 June 2001 calculated by back trajectory using the objective analysis data of the Japan Meteorological Agency. The T_{ice} is also plotted in the figure. The temperature of the air parcels that included the PSCs dropped below T_{ice} about one day before arriving at Syowa Station. The mean cooling rate of the air parcel two days before the arrival was about -5 K/day. Figure 8 shows the back trajectory of the same air parcel of Figure 7. The air parcels were over sea for two days before the arrival. Therefore, the lee waves hardly affected the formation of the observed PSCs in these two days. The average cooling rate of the cooling phase by the inertia gravity wave described in the previous section was about -87 K/day (the amplitude of temperature, ~5 K, divided by one quarter of the period, 5.5/4 h), and was about 18 times larger than that caused by synoptic-scale motion.

[20] The type II PSCs observed at the eastern side of the Scandinavian mountains were formed under the extremely rapid cooling (~-80 K/hour) by lee waves. These PSCs were probably composed of large number of small particles [*Carslaw et al.*, 1998b]. On the other hand, under the relatively slower cooling conditions (less than ~100 degrees per day) in the case of the PSC over Syowa Station,

only a relatively small number of the aerosol particles were nucleated as ice particles, and this smaller number of nucleated particles grew into larger final sizes. Since ice particles formed at the slower cooling rate can grow as large as ~10 μm within an hour [*Toon et al.*, 1989; *Tabazadeh et al.*, 1997], the size of the MPL observed PSC particles possibly be in this size range. The sedimentation velocity of such particles in the lower stratosphere is ~0.01 m/sec. This velocity is smaller than the intrinsic vertical phase velocity (~0.2 m/sec) of the inertia gravity wave. The ice particles formed in the low-temperature regions of waves will move to the upper (higher temperature) side of this region of the phase due to the difference between the sedimentation velocity and the intrinsic phase velocity. Since the ice particles in the size around ~10 μm evaporate within an hour if the atmospheric temperature is higher than T_{ice} [*Toon et al.*, 1989], the particles disappear rapidly compared with the period of the gravity waves.

[21] The inertia gravity waves have the following effects on the formation of the ice PSC particles: if inertia gravity waves are present in the stratosphere where the temperature was already lowered near T_{ice} by synoptic-scale atmospheric motion, the waves additionally lower the temperature at their low-temperature phases. The temperature can be lower than T_{ice-nu} at this region of the phase; the wave thus triggers the formation of the ice particles. Since the cooling rate in this region of particle formation is low, a small number (~0.01 cm^{-3}) of large (~10 μm) particles can be formed through the nucleation process. Since the downward vertical phase velocity is larger than the sedimentation velocity of the particles, and since the particles evaporate rapidly where the atmospheric temperature is higher than the frost point temperature, the vertical structure of the PSC concentration
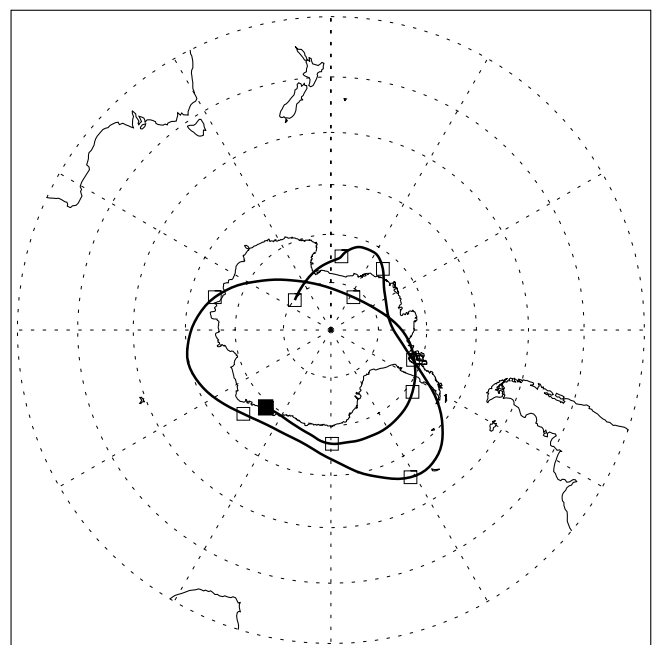
Figure 8. Back trajectory of the air parcel at 20 km over Syowa (solid square) at 1500 LT on 30 June 2001 calculated by using the objective analysis data of the Japan Meteorological Agency. Squares denote 1-day intervals.

is similar to the vertical structure of the low-temperature region due to the waves.

[22] Although the formation of ice PSC particles has been directly observed over the Scandinavian mountain area, the PSC particles formed by lee waves are observed in a limited region downwind of the mountain. On the other hand, inertia gravity waves that originate from various atmospheric instabilities have greater ubiquity. In the Arctic stratosphere the area of cold temperature by synoptic-scale atmospheric motion is often over the ocean. An inertia gravity wave could trigger the formation of the ice particles, as described above.

[23] Since the cooling rate by inertia gravity waves is rather low, the concentration of the formed ice particles is low. Then the concentration of the type I solid particles formed from these ice particles is low, and the size of the type I particles is relatively large. As a result, since the sedimentation velocity of these large particles is high, the nitrate constituents are effectively removed from the stratosphere.

5. Conclusions

[24] Type II PSCs appeared over Syowa, Antarctica when the stratospheric temperature dropped below T_{ice-nu}. It was shown that this low temperature was caused by the dynamic perturbation with inertia gravity waves generated in association with synoptic-scale wave-breaking processes in the upper troposphere. The low-temperature perturbation is needed for the formation of the solid PSC particles. However, since the mechanism of the solid particle formation is still not clear, the main dynamical processes for the perturbation are also not clear, although orographic waves are now thought to be one of the important dynamical processes that cause the perturbation. We have shown a case in which the type II PSCs were formed under the low-temperature perturbation by a nonorographic gravity wave. It was suggested that nonorographic inertia gravity waves of this type can play significant roles in the formation of the solid PSC particles, since the existence of the waves is not limited by the geographical location of high mountains.

References

Carslaw, K. S., et al., Increased stratospheric ozone depletion due to mountain-induced atmospheric waves, *Nature*, *391*, 675–678, 1998a.

Carslaw, K. S., M. Wirth, A. Tsias, B. P. Luo, A. Dörnbrack, M. Leutbecher, H. Volkert, W. Renger, J. T. Bacmeister, and T. Peter, Particle microphysics and chemistry in remotely observed mountain polar stratospheric clouds, *J. Geophys. Res.*, *103*, 5785–5796, 1998b.

Carslaw, K. S., T. Peter, J. T. Bacmeister, and S. D. Eckermann, Widespread solid particle formation by mountain waves in the Arctic stratosphere, *J. Geophys. Res.*, *104*, 1827–1836, 1999.

Fahey, D. W., et al., The detection of large HNO3-containing particles in the winter Arctic stratosphere, *Science*, *291*, 1026–1031, 2001.

Gill, A. E., *Atmosphere-Ocean Dynamics*, 662 pp., Academic, San Diego, Calif., 1982.

Koop, T., H. P. Ng, L. T. Molina, and M. J. Molina, A new optical technique to study aerosol phase: The nucleation of ice from H_2SO_4 aerosols, *J. Phys. Chem. A*, *102*, 8924–8931, 1998.

Lee, H. S., I. H. Hwang, J. D. Spinhirne, and V. S. Scott, Micro Pulse Lidar for aerosol and cloud measurement, in *Advances in Atmospheric Remote Sensing With Lidar*, edited by A. Ansmann et al., pp. 7–10, Springer-Verlag, New York, 1997.

O'Sullivan, D., and T. J. Dunkerton, Generation of inertia-gravity waves in a simulated life cycle of baroclinic instability, *J. Atmos. Sci.*, *52*, 3695–3716, 1995.

Sato, K., An inertial gravity wave associated with a synoptic-scale pressure trough observed by the MU radar, *J. Meteorol. Soc. Jpn.*, *67*, 325–334, 1989.

Sato, K., Sources of gravity waves in the polar middle atmosphere, *Adv. Polar Upper Atmos. Res.*, *14*, 233–240, 2000.

Sato, K., and M. Yamada, Vertical structure of atmospheric gravity waves revealed by the wavelet analysis, *J. Geophys. Res.*, *99*, 20,623–20,631, 1994.

Shibata, T., On the lidar observed sandwich structure of polar stratospheric clouds, II, numerical simulations of externally mixed PSC particles, *J. Geophys. Res.*, *104*, 21,613–21,619, 1999.

Shibata, T., Y. Iwasaka, M. Fujiwara, M. Hayashi, M. Nagatani, K. Shiraishi, H. Adachi, T. Sakai, K. Susumu, and N. Nakura, Polar stratospheric clouds observed by lidar over Spitsbergen in the winter of 1994/1995: Liquid particles and vertical "sandwich" structure, *J. Geophys. Res.*, *102*, 10,829–10,840, 1997.

Shibata, T., K. Shiraishi, H. Adachi, Y. Iwasaka, and M. Fujiwara, On the lidar observed sandwich structure of polar stratospheric clouds, I, implications for the mixing state of the PSC particles, *J. Geophys. Res.*, *104*, 21,603–21,611, 1999.

Shiobara, M., M. Yabuki, H. Kobayashi, T. Shibata, and T. Yamanouchi, Micro-pulse Lidar measurements for cloud and aerosol in the Arctic and Antarctica, in *Proceedings of the Nagasaki Workshop on Aerosol-Cloud Radiation Interaction and Asian Lidar Network, 27-29 November 2001, Nagasaki, Japan*, edited by T. Takamura, pp. 32–35, Cent. for Environ. Remote Sens., Chiba, Japan, 2001.

Solomon, S., Stratpspheric ozone depletion: A review of concepts and history, *Rev. Geophys.*, *37*, 275–316, 1999.

Spinhirne, J. D., Micro pulse lidar, *IEEE Trans. Geosci. Remote Sens.*, *31*, 48–55, 1993.

Sugita, T., Y. Kondo, H. Nakajima, U. Schmidt, A. Engel, H. Oelhaf, G. Wetzel, M. Koike, and P. A. Newman, Denitrification observed inside the Arctic vortex in February 1995, *J. Geophys. Res.*, *103*, 16,221–16,233, 1998.

Swinbank, R. S., and A. O'Neill, A Stratosphere-Troposphere Data Assimilation System, *Mon. Weather Rev.*, *122*, 686–702, 1994.

Tabazadeh, A., O. B. Toon, B. L. Gary, J. T. Bacmeister, and M. R. Schoberl, Observational constraints on the formation of Type Ia polar stratospheric clouds, *Geophys. Res. Lett.*, *23*, 2109–2112, 1996.

Tabazadeh, A., O. B. Toon, and E. J. Jensen, Formation and implications of ice particle nucleation in the stratosphere, *Geophys. Res. Lett.*, *24*, 2007–2010, 1997.

Toon, O. B., R. P. Turco, J. Jordan, J. Goodman, and G. Ferry, *J. Geophys. Res.*, *94*, 11,359–11,380, 1989.

Waibel, A. E., T. Peter, K. S. Carslaw, H. Oelhaf, G. Wetzel, P. J. Crutzen, U. Pöschl, A. Tsias, E. Reimer, and H. Fischer, Arctic ozone loss due to denitrification, *Science*, *283*, 2064–2069, 1999.

Yoshiki, M., and K. Sato, A statistical study of gravity waves in the polar regions based on operational radiosonde data, *J. Geophys. Res.*, *105*, 17,995–18,011, 2000.

Zhang, R., M.-T. Leu, and M. J. Molina, Formation of polar stratospheric clouds on preactivated background aerosols, *Geophys. Res. Lett.*, *23*, 1669–1672, 1996.

————————

H. Kobayashi, Department of Ecosocial System Engineering, Yamanashi University, Takeda 4-3-11, Koufu, Yamanashi 400-8511, Japan. (koba@js.yamanashi.ac.jp)

K. Sato and M. Shiobara, National Institute of Polar Research, 9-10, Kaga 1-chome, Itabashi-ku, Tokyo 173-8515, Japan. (kaoru@nipr.ac.jp; shio@nipr.ac.jp)

T. Shibata, Graduate School of Environmental Studies, Nagoya University, Furo-cho, Chikusa-ku, Nagoya 464-8601, Japan. (tshibata@stelab.nagoya-u.ac.jp)

M. Yabuki, Center for Environmental Remote Sensing, Chiba University, 1-33 Yayoi-cho, Inage-ku, Chiba 263-8522, Japan. (yabuki@ceres.cr.chiba-u.ac.jp)
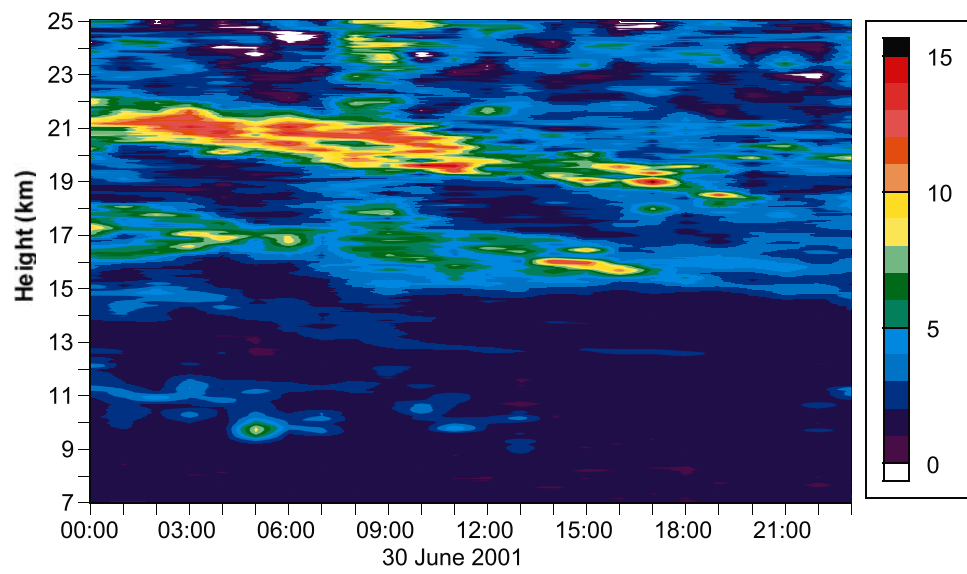
Figure 1. Backscattering ratio by MPL at 523 nm from 00 UT to 23 UT on 30 June 2001.

Figure 6. Time series of horizontal maps of the geopotential height at a pressure level of 215 hPa (contours) and the potential vorticity (PV) at a potential temperature level of 320 K (color), for the time period of 29 June to 2 July 2001, based on UKMO assimilation data. Contour intervals are 100 m. The pressure and potential temperature levels correspond roughly to a height of 10 km. The location of Syowa Station is denoted by a cross.